Dynamics of counterpropagating multipole vector solitons

D. Jović, M. Petrović
Institute of Physics, P.O. Box 57, 11001 Belgrade, Serbia
jovic@phy.bg.ac.yu

M. Belić
Texas A&M University at Qatar, P.O. Box 5825 Doha, Qatar

J. Schröeder, Ph. Jander, C. Denz
Institute of Applied Physics, Westfälische Wilhelms-Universität Münster, Corrensstr. 2/4, D-48149 Münster, Germany

Abstract: Dynamical behavior of counterpropagating (CP) mutually incoherent vector solitons in a 5 x 5 x 23 mm SBN:60Ce photorefractive crystal is investigated. Experimental study is carried out, displaying rich dynamics of three-dimensional CP solitons and higher-order multipole structures, and a theory formulated that is capable of capturing such dynamics. We find that our numerical simulations agree well with the experimental findings for various CP beam structures. Linear stability analysis is also performed, predicting a threshold for the modulational instability of CP beams, and an appropriate control parameter is identified. We attempt at utilizing these results to CP solitons, but find only qualitative agreement with the numerical simulations and experimental findings. However, when broader hyper-Gaussian CP beams are used in simulations, an improved agreement with the theory is obtained.

OCIS codes: (190.5330) Photorefractive nonlinear optics; (190.5530) Pulse propagation and solitons.

References and links

1. S. Trillo, and W. Torruellas eds., *Spatial Solitons* (Springer, New York, 2001).
2. Special Issue on solitons, Ed. M. Segev, Opt. Phot. News **13**, No. 2 (2002).
3. M. Haelterman, A. P. Sheppard, and A. W. Snyder, "Bimodal counterpropagating spatial solitary-waves," Opt. Commun. **103**, 145 (1993).
4. O. Cohen, R. Uzdin, T. Carmon, J. W. Fleischer, M. Segev, and S. Odulov, "Collisions between optical spatial solitons propagating in opposite directions," Phys. Rev. Lett. **89**, 133901 (2002).
5. O. Cohen, T. Carmon, M. Segev, S. Odoulov, "Holographic solitons," Opt. Lett. **27**, 2031 (2002).
6. O. Cohen, S. Lan, T. Carmon, "Spatial vector solitons consisting of counterpropagating fields," Opt. Lett. **27**, 2013 (2002).
7. C. Rotschild, O. Cohen, O.Mandela, T. Carmon, and M. Segev, "Interactions between spatial screening solitons propagating in opposite directions," J. Opt. Soc. Am. B **21,** 1354 (2004).
8. M. Belić, Ph. Jander, A. Strinić, A. Desyatnikov, and C. Denz, "Self-trapped bidirectional waveguides in a saturable photorefractive medium," Phys. Rev. E **68**, 025601 (2003).
9. K. Motzek, Ph. Jander, A. Desyatnikov, M. Belić, C. Denz, and F. Kaiser, "Dynamic counterpropagating vector solitons in photorefractive media," Phys. Rev. E **68**, 066611 (2003).
10. M. Belić, M. Petrović, D. Jović, A. Strinić, D. Arsenović, K. Motzek, F. Kaiser, Ph. Jander, C. Denz, M. Tlidi, and P. Mandel, "Transverse modulational instabilities of counterpropagating solitons in photorefractive crystals," Opt. Express **12**, 708 (2004).
11. Ph. Jander, J. Schröder, C. Denz, M. Petrović, and M. Belić, "Dynamic instability of self-induced bidirectional waveguides in photorefractive media," Opt. Lett. **30**, 750 (2005).
12. M. Petrović, D. Jović, M. Belić, J. Schröder, Ph. Jander, and C. Denz, "Two Dimensional Counterpropagating Spatial Solitons in Photorefractive Crystals," Phys. Rev. Lett. **95**, 053901 (2005).

#9382 - $15.00 USD Received 2 November 2005; revised 9 December 2005; accepted 14 December 2005

13. K. Motzek, M. Belić, T. Richter, C. Denz, A. Desyatnikov, Ph. Jander, and F. Kaiser, "Counterpropagating beams in biased photorefractive crystals: anisotropic theory," Phys. Rev. E **71**, 016610 (2005).
14. J. Schröder, Ph. Jander, C. Denz, T. Richter, K. Motzek, and F. Kaiser, "Counterpropagating dipole-mode vector soliton," Opt. Lett. **30**, 1042 (2005).
15. C. Denz, M. Schwab, and C. Weilnau, *Transverse pattern formation in photorefractive optics* (Springer, Berlin, 2003).
16. M. Schwab, C. Denz, and M. Saffman, "Transverse modulational instability in counterpropagating two-wave mixing with frequency-detuned pump beams," J. Opt. Soc. Am. B **18**, 628 (2001).
17. J. B. Geddes, R. A. Indik, J. V. Moloney, and W. J. Firth, "Hexagons and squares in a passive nonlinear optical system," Phys. Rev. A **50**, 3471 (1994).
18. O. Sandfuchs, F. Kaiser, and M. Belić, "Self-organization and Fourier selection of optical patterns in a nonlinear photorefractive feedback system," Phys. Rev. A **64**, 063809 (2001).

1. Introduction

Spatial solitons - self-trapped beams of light propagating without change in a diffractive nonlinear medium - have become much investigated topics of research in nonlinear optics [1], owing to their novel physics and potential applications. Envisioned for applications in all-optical information processing, they come in a variety of forms - as bullets, screening, quadratic, photovoltaic, and lattice solitons, or as bright, dark, and grey [2]. They are generated in different media, by different nonlinear mechanisms, but the self-focusing effect, produced by light-induced changes in the medium's index of refraction, appears as the common thread in all mechanisms. Self-focusing in photorefractive (PR) crystals is achieved through the generation of space charge field, which is caused by the photo-induced redistribution of charges that modifies the index of refraction. Application of an external DC electric field across the crystal and an additional uniform illumination are found necessary for a more effective soliton formation process.

Thus far the formation and interactions of spatial screening solitons have been studied mostly in the copropagation geometry, with a few exceptions [3-7]. In these references the counterpropagating (CP) solitons were considered theoretically in one transverse dimension (1D), in Kerr and local PR media, and in the steady state. No dynamical effects were presented. In Refs. [8-10] we studied numerically the two-dimensional (2D) CP vector solitons and displayed some novel dynamical beam structures in PR crystals. In Ref. [11, 12] we reported the first experimental evidence of CP spatial solitons, and discovered dynamic instabilities in their behavior. We also improved on the commonly used local isotropic theory of incoherent CP beam mixing in PR crystals, by formulating a general anisotropic theory of coherent mixing [13].

Here we present further experimental evidence for the existence and interactions of 2D CP vector solitons and higher-order multipole self-trapped optical structures in a PR crystal, and investigate theoretically and numerically the splitup transitions and dynamical instabilities of such structures. We restrict our attention to the single CP vector solitons, dipole-mode and dipole-dipole beam arrangements. All three arrangements are found to display transverse splitup instabilities, however the dipole-mode [14] and the dipole-dipole cases provide for the dynamically more stable beam structures than the single CP solitons, under similar conditions. We apply linear stability analysis (LSA) to the CP beam configurations at hand, in an attempt to explain the splitup instability of CP solitons as a symmetry-breaking first-order phase transition, and undertake to identify appropriate control parameters. Experimental observations are found to be in good agreement with the numerical simulations of CP beams, with a time-dependent nonlinearity, however the results of LSA, as applied to CP solitons, turned up in need of further improvement. To verify our results of LSA, and to validate our numerical algorithm, we utilize broader hyper-Gaussian beams in numerical simulations, in order to display and compare with ordinary modulational instabilities (MI) and pattern formation of CP beams [15]. In this case an improved agreement with LSA is obtained.

In Sec. 2 of the paper we describe the experiment. Section 3 introduces the model. In Sec. 4 we provide for a comparison between experimental and numerical results. Linear

#9382 - $15.00 USD Received 2 November 2005; revised 9 December 2005; accepted 14 December 2005

stability analysis is performed in Sec. 5 and the threshold results are compared to the numerical in Sec. 6. Section 7 contains a brief look into the modulational instabilities of broader hyper-Gaussian beams. Section 8 brings conclusions.

2. Experiment

The study of CP beams is conducted in the experimental setup of Fig. 1. Laser beam, derived from a frequency-doubled Nd:YAG laser emitting at *532 nm*, is split and focused onto the opposite faces of a photorefractive SBN60:Ce crystal (*5 x 5 x 23 mm*^{3}), along one axis. The total beam power is about *2* μ*W*. The beam components are made incoherent in the medium by reflecting one component off the mirror mounted on a vibrating piezo-crystal. The *c* axis of the PR crystal is along one of the *5 mm* edges, so that by rotation both the *23 mm* axis and the other *5 mm* axis can be used as propagation directions of the beams. To exploit the large electro-optic component $r_{33} \approx 200$ *pm/V* of our SBN sample, the incident laser beams are linearly polarized parallel to the c axis, perpendicular to the propagation direction. A DC electric field of the order of *1 kV/cm* is applied across the crystal, along the c axis, and the crystal is illuminated by a uniform white light, to create artificial dark conductivity. The strength of the applied field is used to fine-tune the coupling constant between beams.

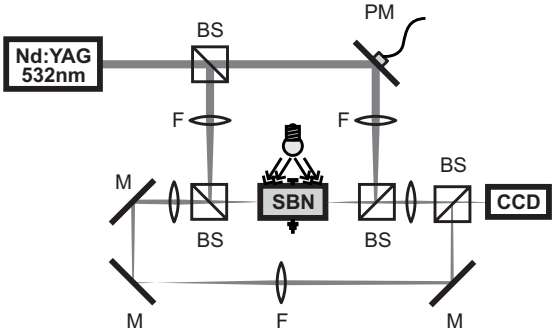

Fig. 1. Experimental setup for the investigation of CP solitons. BS: beam splitters, PM: vibrating piezo-mirror, SBN: Strontium-Barium-Niobate crystal.

Stable CP solitons are readily observed over the *5 mm* propagation distance, with an applied field of *1.3 kV/cm* and the initial beam peak intensity about twice the background intensity. Incoherent Gaussian beams of *20* μ*m* FWHM are launched head-on, and both the forward and the backward propagating beams self-focus within a few seconds into a CP soliton of *~ 20* μ*m* FWHM, tightly overlapping. When the propagation distance is increased from *5 mm* to *23 mm*, for identical other conditions, a completely different dynamical behavior is observed. The beams still self-focus approximately into solitons, but they do not overlap anymore. At the exit face most of the beam intensity is expelled to a transversely shifted position (about 1 beam width), while a fraction of the beam remains guided by the other beam. We call this the splitup transition. The beams remain steady at the new positions, or oscillate about. At higher beam couplings (higher applied voltage) the exit beam spots start to rotate and execute more complex dynamics about the input beam positions. We did not vary the input beam intensities, other than to keep it in the region of soliton existence. At high, or at very low beam intensities above background, the solitons cease to exist. Owing to the saturable nature of nonlinearity, there exists a window in intensities, in which the CP solitons can be observed.

3. The model

To understand the behavior of CP vector solitons we formulated a time-dependent model for the formation of self-trapped CP optical beams [8], based on the theory of PR effect. The model consists of wave equations in the paraxial approximation for the propagation of CP

#9382 - $15.00 USD Received 2 November 2005; revised 9 December 2005; accepted 14 December 2005

beams and a relaxation equation for the generation of space charge field in the PR crystal, in the isotropic approximation. The model equations in the computational space are of the form:

$$i\partial_z F = -\Delta F + \Gamma E F \ , \tag{1}$$

$$-i\partial_z B = -\Delta B + \Gamma E B \ , \tag{2}$$

$$\tau\partial_t E + E = -\frac{I}{1+I}, \tag{3}$$

where F and B are the forward and the backward propagating beam envelopes, Δ is the transverse Laplacian, Γ is the dimensionless coupling constant, and E the homogenous part of the space charge field. The relaxation time of the crystal τ also depends on the total intensity, $\tau=\tau_0/(1+I)$. The quantity $I=|F|^2+|B|^2$ is the laser light intensity, measured in units of the background intensity. A scaling $x/x_0 \rightarrow x$, $y/x_0 \rightarrow y$, $z/L_D \rightarrow z$, is utilized in writing the propagation equations, where x_0 is the typical FWHM beam waist and L_D is the diffraction length. The assumption, appropriate to the experimental conditions at hand, is that the counterpropagating components interact only through the intensity-dependent space charge field. To make matters simple, we did not account for the temperature (diffusion) effects, although they are found to influence the interaction of CP beams [7]. In experiment these effects were compensated by focusing the input B beam at the place of the exit and in the direction of the output F beam.

The propagation equations are solved numerically, concurrently with the temporal equations, in the manner described in Ref. [10] and references cited therein. The dynamics is such that the space charge field builds up towards the steady state, which depends on the light distribution, which in turn is slaved to the change in the space charge field. As it is seen, this simple type of dynamics does not preclude a more complicated dynamical behavior. Some of our numerical results are presented concurrently with the experimental results in Figs. 2 – 5. It is seen that the numerics agrees, at least qualitatively, with the experiment.

A more tricky problem is to provide for an explanation of the nature and the cause of the transverse splitup instability. In Refs. [9, 10] we presented a simple theory of beam displacement - derived in two independent ways - that can account for such transverse shifts. We attempt here at utilizing the standard theory of modulational instabilities (MI), to obtain a threshold curve for the CP beams splitup that at least qualitatively agrees with the experimental and numerical results. In doing so, we are aware of the fact that, although both are symmetry breaking phenomena, the pattern forming MI represents a spontaneous breaking of the translational symmetry of a homogeneous state, whereas the splitup transition is the breaking of the rotational symmetry of an isolated CP soliton. Thus, MI involves the appearance of transverse waves at a critical value of k_c, whereas the splitup instability involves a jump of the peaked structure in the transverse inverse space at some value of k_c. These two values of k_c might, but need not be connected.

4. Comparison between experiment and numerics

The aim of our numerical simulations is to qualitatively capture the most prominent experimental findings, using a simple theoretical model and a tractable numerical method. To this end we employ an isotropic model without temperature (diffusion) effects. Although the experiment is performed on an anisotropic crystal at a finite temperature, an effort is exerted to minimize the effects of anisotropy and diffusion. Thus, the geometry of beam coupling and the use of incoherent beams helped reducing the differences between the isotropic and anisotropic interactions in the crystal [13]. Also, an attempt is made in experiment to compensate for the diffusion effects, by focusing the backward input beam at the place of exit and in the direction of the output forward beam. The end result is that our numerical simulations closely resemble experimental results concerning the stable CP solitons and single splitup transitions of CP beams, including the size and the direction of transverse

#9382 - $15.00 USD Received 2 November 2005; revised 9 December 2005; accepted 14 December 2005

displacements. Nonetheless, the experiment still shows the influence of the preferential (*c*) direction and of the beam bending, which was found to affect the interaction of CP beams [7].

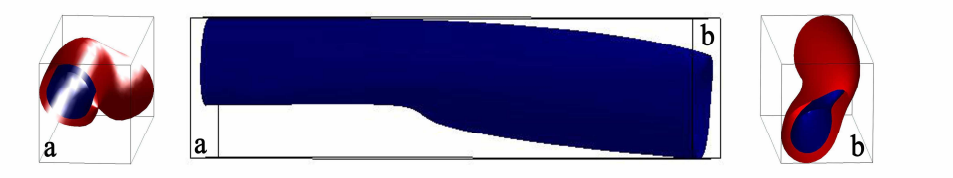

Fig. 2. Isosurface plots of a CP soliton after a splitup transition. Forward propagating component is displayed in the steady state, (a) View along the entrance face of the crystal, (b) View along the exit face of the crystal. Simulation parameters: $|F_0|^2=|B_L|^2=0.6$, $\Gamma=7.17$, $L=5.75L_D=23$ *mm*, and initial beam widths (FWHM) are *20* μm.

Both the forward and the backward components are found to deflect to the same side. Unstable regions are reached upon increasing the thickness of the crystal and the coupling constant, in both experiment and simulations. In addition, in numerics we also varied the intensity of input laser light. Dynamical behavior in numerical simulations qualitatively follows that of the experimental runs. Typically output beam spots rotate about the input beam positions, or rapidly pass through them, until stable displaced equilibrium positions are found. Then they oscillate about these positions. In the case no equilibrium is found, the output beams continue to dance about the input beams indefinitely.

Concerning the single splitup transition, in numerics we observe the behavior close to the one in experiment. Hence, in Fig. 2 we present a numerical example only. It is seen that the beams bend, elongate, and split into two. Most of the beam intensity is focused to a new transverse position. The direction of the transverse displacement is approximately in the direction of the external field or the *c* axis, which is horizontal here.

When the coupling constant is increased, the transient dynamics lasts even longer, to the point that steady state is not reached over the duration of experiment (up to 3 hours). The dynamics is such that the exiting beam rotates around or passes through the input beam, or dances irregularly about it. All these dynamical phases could qualitatively be reproduced by numerical simulation (Fig. 3). As it can be seen in the movies 3(b), (c), a localized peaked structure in the direct space forms a localized peaked structure in the inverse space, and their dynamics is correlated. In fact, one initially observes a faint ring in the inverse space and then most of the beam intensity focuses to a point.

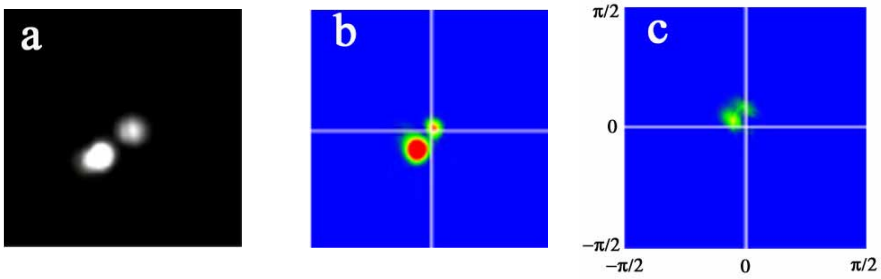

Fig. 3. Movies of the Gaussian-Gaussian beam interaction: (a) Exit face of the crystal, experimental (2.031 MB). (b) The corresponding numerical simulation of the backward beam (at the exit face of the crystal), in the direct space (878 KB), (c) in the inverse space (858 KB). Parameters are as in Fig. 2, except for $|F_0|^2=|B_L|^2=7.5$.

In addition to head-on colliding CP solitons, we also investigate, experimentally and numerically, the dipole-mode [14] and the dipole-dipole vector CP solitons. In the case of dipole-mode CP solitons (Fig. 4), a fundamental Gaussian beam is counter-propagated to a dipole beam, located midway between the two out-of-phase dipole components, which are

#9382 - $15.00 USD Received 2 November 2005; revised 9 December 2005; accepted 14 December 2005

aligned perpendicular to the external field. A transverse splitup occurred over the *23 mm* propagation distance. Again, the experimental observation of dynamical behavior is in qualitative agreement with the numerical simulations. Notice that the direction of the *x* axis is reversed in the experimental movie for the fundamental mode component intensity, because in the experiment one is looking at the face of the crystal from the opposite direction.

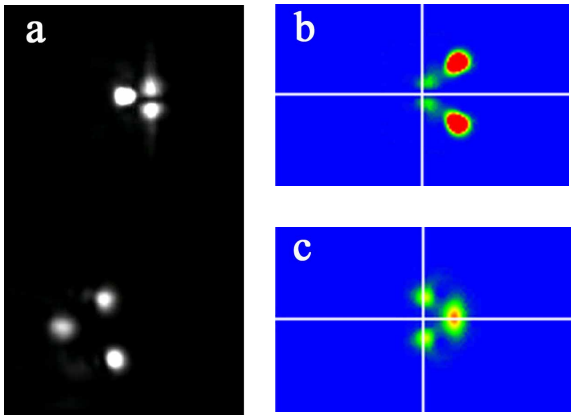

Fig. 4. Movies of the dipole-mode beam interaction. (a) Experiment: The upper frame presents the exit face of the crystal for the dipole component, the lower frame presents the exit face for the fundamental mode component (2.818MB). (b) Movie of the dipole (592 KB), and (c) movie of the fundamental mode component (502 KB), from the corresponding numerical simulation. They are presented at their own exit faces, looking in the forward propagation direction. Parameters are as in Fig. 2, except for $|F_0|^2 = |B_L|^2 = 4$. Initial distance between dipole partners is *40 μm*.

The next configuration investigated was the dipole-dipole vector CP soliton (Fig. 5). In the case of dipole-dipole CP solitons, two identical dipoles with the components out of phase are counterpropagated head-on. The dipoles are aligned perpendicular to the external field, which always points in the horizontal direction. A transverse splitup occurs again. The direction of the splitup is preferentially along the direction of the external field, and it also depends on the added noise (Fig. 5(b)). Only in the case when some noise is added to one of the beams are we able to observe skewed splitups, and achieve better agreement with the experiment, but the dipole oscillates all the time. For the case with no noise (Fig. 5(c)), in the beginning we notice oscillations along the *y* axis, and after a short time these oscillations are damped. Compared to the single CP soliton cases, the cases involving dipoles are more stable and the transient dynamics last shorter.

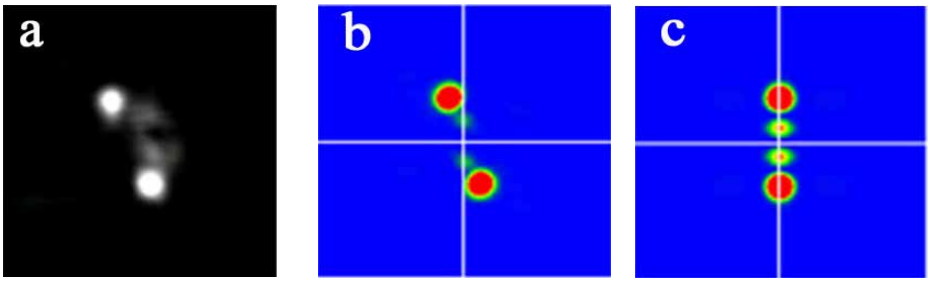

Fig. 5. Movies of the dipole-dipole interaction. (a) Experiment: the forward beam (upper) and backward beam (lower), at the exit face of the crystal (2.818 MB). The corresponding numerical simulations of the backward beam: (b) with an extra noise of *5%* added to the input beam intensity (902 KB), (c) without noise (426 KB). Parameters are as in Fig. 4, except for $|F_0|^2 = |B_L|^2 = 1.3$.

#9382 - $15.00 USD Received 2 November 2005; revised 9 December 2005; accepted 14 December 2005

5. Linear stability analysis

In the standard MI theory one follows the dynamics of weak perturbation to a wave and looks for instances of exponential growth of the perturbation. Such a growth promotes the amplification of sidebands and leads to the appearance of localized transverse structures. This approach is used much in the theory of transverse optical patterns [15]. Here however, the whole object - a CP soliton - undergoes a sudden transverse shift to a new position. We suppose that at the threshold the critical wave vector of the unstable ring in the transverse k space will focus to a spot, to which most of the energy (intensity) of the initial beam will be transferred. As mentioned, the assumption is that a localized peaked structure in the direct space will form a localized peaked structure in the inverse space, and that their dynamics will be correlated. This expectation is borne in numerical simulations.

In the steady state we have a plane wave solution:

$$F_0(z) = F_0(0)\exp(-i\Gamma E_0 z)\,, \tag{4}$$

$$B_0(z) = B_0(L)\exp(i\Gamma E_0 (z-L))\,, \tag{5}$$

where $E_0 = -\, I_0/(1+I_0)$. In this case I_0 is a conserved quantity (it does not depend on z), so E_0 also does not depend on z.

The primary threshold is determined by the linear instability of the steady-state plane-wave field amplitudes F_0 and B_0, and the homogenous part of the space charge field E_0. In order to carry out linear stability analysis we make a change of variables to a basis most convenient to display the structure and symmetries of the problem. The time and space evolution of the perturbations f, b and e, is introduced by an ansatz:

$$F = F_0(1+f)\,, \tag{6}$$

$$B = B_0(1+b)\,, \tag{7}$$

$$E = E_0(1+e)\,, \tag{8}$$

along with the boundary conditions:

$$f(0) = b(L) = 0\ . \tag{9}$$

Neglecting higher harmonics and terms quadratic in f, b, and e, and following the procedure described in Ref. [16], we obtain the final form of the threshold condition:

$$\begin{aligned} &1+\cos(k^2L)\cos(\sqrt{k^4L^2-4A\Gamma k^2L^2})+\\ &\frac{(k^2L-2A\Gamma L)}{\sqrt{k^4L^2-4A\Gamma k^2L^2}}\sin(k^2L)\sin(\sqrt{k^4L^2-4A\Gamma k^2L^2}) = 0 \end{aligned} \tag{10}$$

The threshold equation has the same form as the threshold condition in Ref. [17]:

$$2+2\cos(\Psi_1)\cos(\Psi_2)+\left(\Psi_1/\Psi_2+\Psi_2/\Psi_1\right)\sin(\Psi_1)\sin(\Psi_2) = 0\,, \tag{11}$$

where $\Psi_1 = k^2L$, $\Psi_2 = \sqrt{k^4L^2-4A\Gamma k^2L^2}$, and we choose $|F_0|^2=|B_L|^2$, so that $A = |F_0|^2/(1+2|F_0|^2)^2$. The problem treated in Ref. [17] is the counterpropagation in Kerr media, so that the form of Ψ's is different. The same form of the threshold condition should

#9382 - $15.00 USD Received 2 November 2005; revised 9 December 2005; accepted 14 December 2005

not be surprising, because it originates from the CP geometry used in both papers. The symmetry of the problem here is more important than the particular form of the nonlinearity.

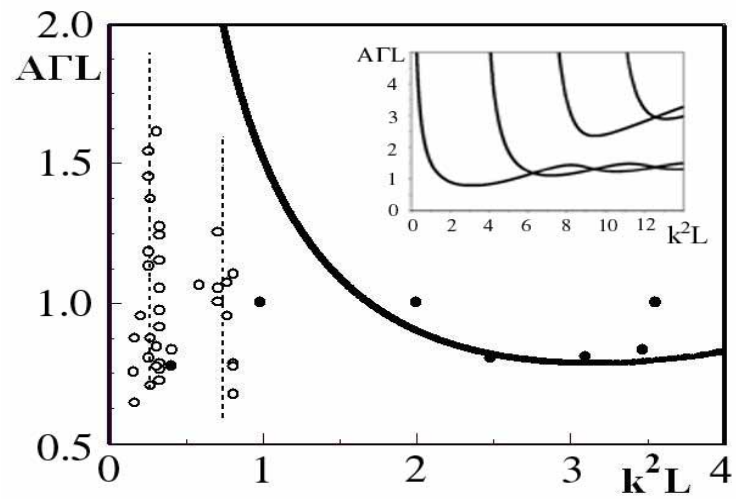

Fig. 6. Threshold curves obtained from Eq. (11). Inset provides an extended view. Two clusters of open-circled points, obtained numerically, represent jumps in k^2L of the peaked soliton-like structures in the inverse space. Dashed lines are the average values of k^2L for the two sets of points. Filled circles represent points where the broader hyper-Gaussian CP beams undergo MI.

Owing to the transcendental nature of Eq. (11) there exist an infinite number of neutral stability curves [17]. Since Eq. (11) can be factorized

$$H_1 H_2 = 0\,, \tag{12}$$

these curves split into two groups. The function H_1 is defined by:

$$H_1(\Psi_1, \Psi_2) = \frac{\Psi_1}{\Psi_2}\sin(\Psi_1/2)\sin(\Psi_2/2) + \cos(\Psi_1/2)\cos(\Psi_2/2) \tag{13}$$

and $H_2(\Psi_1, \Psi_2) = H_1(\Psi_2, \Psi_1)$. One group of threshold curves is defined by $H_1=0$, and the other group by $H_2=0$. They cross when $H_1=H_2=0$. The crossing points are found when both Ψ_1 and Ψ_2 are the integer multiples of π, say $m\pi$ and $n\pi$, where one of the m, n must be even and the other odd. The location of crossing points is given by:

$$A\Gamma L = \frac{(m^2 - n^2)\pi^2}{4k^2 L}\,, \tag{14}$$

$$k^2 L = m\pi\,. \tag{15}$$

$A\Gamma L$ is the smallest for $m=n+1$, and larger differences ($m=n+3\ldots$) give higher-order modes. Hence, there are three control parameters in the problem: Γ, L and the input beam intensity, conveniently combined into one control parameter of the form $A\Gamma L$. For small values of Γ and L stable soliton propagation is observed, whereas for higher Γ and L unstable behavior is seen [8,9]; the dependence on I, which figures in A, is more complicated.

It is difficult to compare experimental and numerical results with the general threshold curves, presented in Fig. 6. For comparison, three clusters of points, obtained numerically, are also plotted in Fig. 6. The two clusters to the left (open circles) depict how much the peaked structures in the inverse space jump transversally after a splitup transition. Each point represents a CP structure, with a specific value of $A\Gamma L$, after a jump in the k space, and in the steady state. It is seen that the points group themselves about two values of $k_c^2 L$ (*~0.27* and

#9382 - $15.00 USD Received 2 November 2005; revised 9 December 2005; accepted 14 December 2005

~*0.73*, the vertical dashed lines) which are way below the expected value of $k_c^2 L$ (~*3.14*) for the critical ring of MI modes. This is not difficult to understand, in view of the fact that the displaced soliton is a large-scale primary structure, whereas MI represents a side-band secondary wave pattern. Also, the values of the order parameter $A\Gamma L$ range between *0.63* and *1.6*, whereas the critical MI value equals $\pi/4$. There is but a qualitative agreement between LSA and numerical results. However, the agreement improves significantly if, instead of solitons, one considers broader hyper-Gaussian beams [18]. The third set of points in Fig. 6 (filled circles) represent the threshold points of MI instabilities of a few such hyper-structures (of the order 4). It is found that the threshold points of narrower beams fall closer to the splitup points of CP solitons, whereas the points of broader beams (FWHM=*150* μm in the figure) fall closer to the threshold curve.

6. Threshold curves and numerics

Because there are two values of $|F_0|^2$ for each value of *A*, we consider the threshold intensity as a function of the square of the transverse wave vector (Figs. 7(a), 8(a), and 9(a)). Then for each pair of Γ and *L* we have different threshold curves. An analysis of Eq. (11), for given Γ and *L*, gives an extra condition:

$$k^2 < \frac{\Gamma}{2}, \tag{16}$$

which means that k^2 is not arbitrary large, as it might seem from Fig. 6.

Figures 7 – 9 display our results concerning the threshold behavior of CP beams during the development of MI. Also provided in Figs. 7(a), 8(a) and 9(a) are the arrows which depict how much the CP solitons jump transversely in the *k* space in numerical simulations, after a splitup transition. There may be more than one splitup transition, one following the other. After two splitups one usually observes a disordered motion of the beam spots. The left end of an arrow points to the value of k^2 of the peak intensity in the steady-state, the right end points to the maximum value of the total transient change in k^2. The end points are calculated by independent numerical runs of the full simulations. In fact, the left-end points of many runs are collected and displayed in Fig. 6. In the case no steady-state is found, only the maximum value of the total transient change in k^2 is displayed, represented by a dot (Figs. 8 and 9).

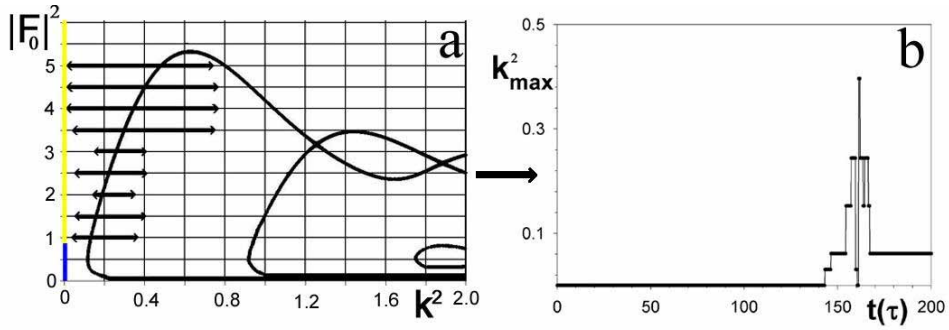

Fig. 7. (a) Threshold intensity $|F_0|^2$ versus the square of the transverse wave vector k^2, for $\Gamma=4$ and $L=5L_D$. Blue color represents the intensity region with stable solitons, yellow represents the intensity region with splitup(s). (b) The square of the transverse wave vector (k^2_{max}) corresponding to the maximum value of the far-field intensity versus time, for $|F_0|^2=2.5$. Steady state is reached.

For the control parameters $\Gamma=4$ and $L=5L_D$ (Fig. 7), besides stable solutions only one and two splitup transitions are observed. It is seen that the arrows provide a qualitative agreement with the form and the position of the lowest branch of the threshold curve. It is difficult to observe higher order transitions, because of the intervening dynamical effects. The double-valued form of the functions in Fig. 7(a) is the signature of a first-order phase transition: the

#9382 - $15.00 USD Received 2 November 2005; revised 9 December 2005; accepted 14 December 2005

bottom parts of the curves are unobservable, and for a transition to occur a small but finite value of the initial intensity is necessary. Also, above the highest hump of the threshold curves no transitions are observed. In fact, at such high intensities, experimentally no CP solitons are seen. They can exist only in a certain window of beam intensities. From Fig. 7(b) we see that the single splitup at $t=160\ \tau$ corresponds to a short damped oscillation in the inverse space, before the steady state is reached.

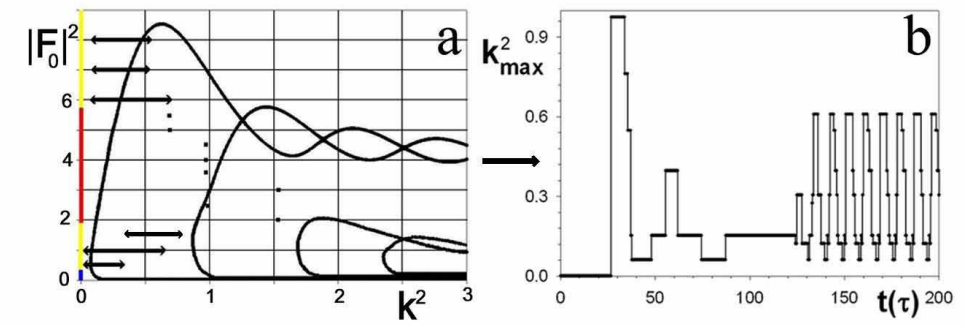

Fig. 8. (a) Threshold intensity $|F_0|^2$ versus the square of the transverse wave vector k^2, for $\Gamma=6$ and $L=5L_D$. Colours have the same meaning as in Fig. 7(a), red represents the intensity region of unstable behavior, where the steady state is never reached. (b) The square of the transverse wave vector corresponding to the maximum value of the far-field intensity (k^2_{max}) versus time, for $|F_0|^2=4$. After a transient, a limit cycle is reached.

For a slightly higher coupling strength $\Gamma=6$ (Fig. 8), there are two intensity regions where the threshold curves cross each other. The most stable are the beams with intensities lying outside those two regions. In Figs. 7(a) and 8(a), the maximum transverse jump in the k space evidently complies with the condition in Eq. (16). Fig. 8(b) depicts situation in the unstable cross-over region, where a more complicated behavior is expected. A transient splitup transition is noted that lasts from $t=30\ \tau$ to $t=60\ \tau$, and after $t=130\ \tau$ the system starts displaying regular oscillation in the first quadrant of the transverse plane. A limit cycle is reached. This behavior, however, is unrelated to Fig. 8(a), in which a steady-state situation is presented.

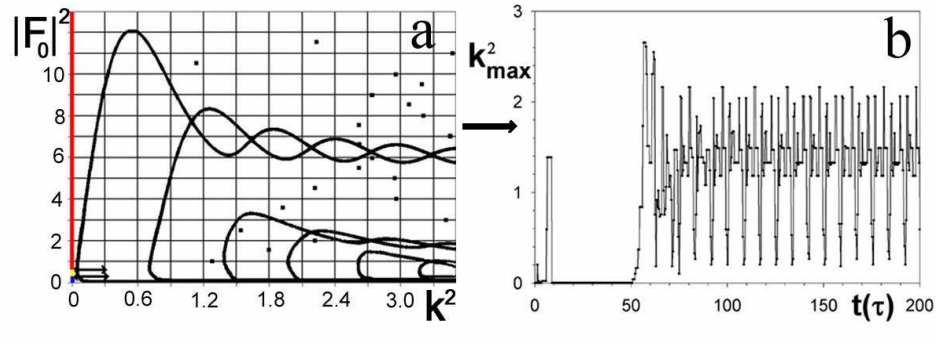

Fig. 9. (a) Threshold intensity $|F_0|^2$ versus the square of the transverse wave vector k^2, for $\Gamma=7.17$ and $L=5.75L_D$. Colours have the same meaning as in Fig. 8(a). (b) The square of the transverse wave vector (k^2_{max}) corresponding to the maximum value of the far-field intensity versus time, $|F_0|^2=7.5$. Irregular behavior is observed.

When $\Gamma=7.17$ and $L=5.75L_D$ (Fig. 9), as in one of the experiments, a complicated dynamical behavior is observed, especially in the region of intensities where the threshold curves cross each other and where the influence of the saturable nonlinearity is the largest.

#9382 - $15.00 USD Received 2 November 2005; revised 9 December 2005; accepted 14 December 2005

This is the region of the most unstable behavior, with the highest displacement in k^2. Below and above this region the dynamics is simpler. In the case where steady-state is never reached, there is only the maximum value of the total transient change in k^2. The case presented in Fig. 9(b) corresponds to the movie 3(c), as all control parameters (including the intensity) are the same. An irregular dynamics of the beam spots is observed, both experimentally and numerically. For the experimental conditions, we can see splitup transitions only for relatively small values of the intensities, and the arrows are then in a qualitative agreement with the threshold curve branch with the minimal value of k^2. Nevertheless, the threshold analysis fails to adequately describe numerical and experimental findings; Figs. 9(a) and 9(b) are essentially unrelated to each other. Still, Figs. 7(b), 8(b) and 9(b) conveniently depict how the temporal signal k^2 acquires a more complex behavior, changing from the fixed point, to the limit cycle, and finally to the quasiperiodic motion, as the driving parameter ΓL increases.

For the case presented in Fig. 9(a), when the input intensity is $|F_0|^2=12$, the transverse jump in the k space in numerical simulations is greater than the greatest possible, according to Eq. (16) (the corresponding dot is not shown on the graph). This means that the linear stability analysis is definitely unable to appropriately describe the behavior at high values of Γ and L. However, as mentioned, when broad hyper-Gaussian beams are used, instead of narrow Gaussian beams, regular modulational instabilities appear, and their onset is in good agreement with the threshold curves. A few examples of such behavior are presented in Figs. 10 and 11.

7. Broad hyper-Gaussian beams

The consideration of broader hyper-Gaussian beams offers rich opportunities for observing complex pattern-forming dynamical behavior. We should again stress the fact that our splitup transitions do not appear to be of this common type of MI. The solitons themselves could be considered as related to the filaments of MI, and, as such, should be stable against the same kind of MI. Nonetheless, it is still of interest to explore the cross-over region by increasing the size of solitonic beams, until they display MI, and to compare it to the splitup transition.

Figure 10 represents the modulational instability of CP hyper-Gaussian beams of FWHM=$150\ \mu m$, obtained numerically. After a few integration cycles, the rings in the beam structure appear, in the direct as well as in the inverse space. The radius of this initial ring is plotted in Fig. 6, as one of the filled circles to the right. The structure never reaches steady state, for the duration of the integration. What might be of interest here is that the structure undergoes a series of symmetry breaking changes, starting from an O(2) symmetry at $t=0$, going through a C_{4v} point symmetry at $t=80\ \tau$, and ending with an asymmetric C_1 state. This last transition apparently is the analogue of the splitup transition of CP solitons.

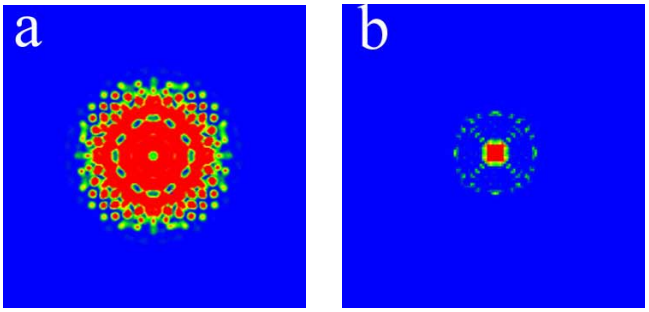

Fig. 10. Movies of modulational instabilities of a broad hyper-Gaussian beam, for the backward component. (a) (1999 KB) Direct space (7293 KB version), (b) (1763 KB) Inverse space. The order of the hyper-Gaussian is 4, FWHM=$150\ \mu m$, other parameters: $\Gamma=27.6$, $L=0.5L_D$, $|F_0|^2=|B_L|^2=3$.

Patterns forming in MI of broader beams can also acquire a more ordered appearance. Two such cases are presented in Fig. 11, one depicting a steady-rotating hexagonal CP beam

#9382 - $15.00 USD Received 2 November 2005; revised 9 December 2005; accepted 14 December 2005

structure, and the other an almost stationary transverse pattern of octagonal symmetry. The only difference between the two cases is the width of the incident beams; in the first case it equals *100 μm*, in the second *150 μm*. All other parameters are the same. The rotating hexagon is interesting in the sense that a quasi-stable symmetric two-ring hexagonal structure breaks its central symmetry at about *$t=50\ \tau$*, and then starts to rotate. This behavior is characteristic of patterns going through a Hopf bifurcation [15]. Also, the beams acquire net angular momentum, which they did not possess to start with. Systems undergoing point symmetry breaking transitions need not conserve angular momentum. An interesting feature in the octagonal pattern is that it also contains octagonal and square patterns of higher order. The mixing and competition of patterns, as well as the appearance of defects and domain-walls, are common features of pattern formation in PR media [15].

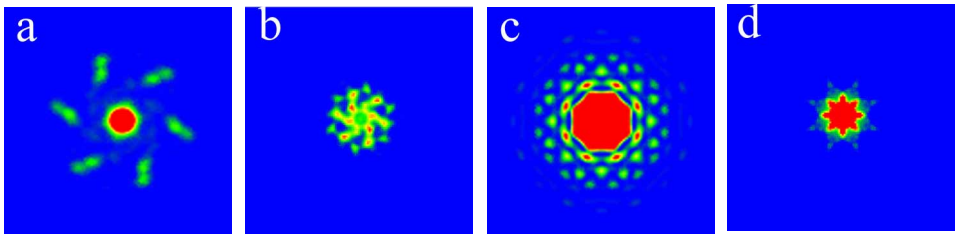

Fig. 11. Movies of the modulational instabilities of hyper-Gaussians, resulting in a rotating hexagon, (a) (805 KB) direct space, (b) (1719 KB) inverse space intensity distributions (2637 KB), and in a steady-state octagonal pattern, (c) (1640 KB) direct space, (d) (1008 KB) inverse space intensity distributions. The parameters for both cases are the same, $\Gamma=16.14$, $L=3L_D$, $|F_0|^2= |B_L|^2=5$, the only difference is the beam widths: *100 μm* in the first, and *150 μm* in the second case.

8. Conclusions

In summary, we reported on the experimental observation of the three-dimensional counter-propagating spatial vector solitons in a photorefractive crystal, including the more complex dipole-mode and dipole-dipole interaction geometries. A peculiar dynamic behavior of CP solitons is observed, in that the counterpropagating components suddenly change their transverse positions, and from an attracting interaction switch to repelling. Previously stable equilibrium becomes a limit cycle, the behavior suggesting of a Hopf bifurcation happening in the system. Using a simple model, we explain this behavior as a spontaneous symmetry breaking first order phase transition, and identify the appropriate control parameter(s). We also observe rich dynamics of the three-dimensional counterpropagating solitons and formulate a theory capable of capturing such dynamics. We obtain good agreement, even when considering dynamics in detail, between the numerical simulations and the experimental results. We perform linear stability analysis, to try to confirm experimental and numerical findings concerning the threshold behavior. In this case only qualitative agreement between numerical and LSA results is obtained for CP solitons, which however can be improved by considering broader CP hyper-Gaussian beams. A few examples of the standard modulational instabilitiy of broad CP beams are also presented.

Acknowledgments

Work at the Institute of Physics is supported by the Ministry of Science and Environment Protection of the Republic of Serbia, under the project OI 1475. Part of this work was supported by the Deutsche Forschungsgemeinschaft.

#9382 - $15.00 USD Received 2 November 2005; revised 9 December 2005; accepted 14 December 2005